

Experimental evidence of high-resolution ghost imaging and ghost diffraction with classical thermal light

D. Magatti, F. Ferri, A. Gatti, M. Bache, E. Brambilla, and L.A. Lugiato

INFN, Dipartimento di Fisica e Matematica, Università dell'Insubria, Via Valleggio 11, 22100 Como, Italy

(Dated: September 13, 2018)

High-resolution ghost image and ghost diffraction experiments are performed by using a single source of thermal-like speckle light divided by a beam splitter. Passing from the image to the diffraction result solely relies on changing the optical setup in the reference arm, while leaving untouched the object arm. The product of spatial resolutions of the ghost image and ghost diffraction experiments is shown to overcome a limit which was formerly thought to be achievable only with entangled photons.

PACS numbers: 42.50.Dv, 42.50-p, 42.50.Ar

The ghost imaging protocol, provides a flexible way of performing coherent imaging by using spatially incoherent light. It relies on the use of two spatially correlated beams, one of them illuminating an object, while the other holds a known reference optical setup. Information on the object spatial distribution is obtained by correlating the spatial distributions of the two beams. Traditionally parametric down-conversion (PDC) is the source of the correlated beams. In the low-gain regime single pairs of entangled signal-idler photon can be resolved, and the information is extracted from coincidence measurements [1, 2, 3, 4, 5], while in the high-gain regime several photon pairs form entangled beams and the information is contained in the signal-idler intensity correlation [6, 7, 8, 9]. Landmark experiments in the low-gain regime showed that using entangled photons both the object image could be retrieved (the “ghost image” experiment [1]) as well as the object diffraction pattern (the “ghost diffraction” experiments [2, 3]).

Recently, a very lively debate arised, aiming to identify which aspects (if any) of ghost imaging truly requires entanglement and which could be reproduced by using classically correlated sources. The first theoretical interpretation of the experiments suggested that entanglement of photon pairs was essential to retrieve information from the correlations[4, 5]. This interpretation was challenged both by theoretical arguments [6] and experiments [11, 13], which showed that virtually any single result of ghost imaging could be reproduced by using classical sources with the proper kind of spatial correlation. However, theoretical investigations showed that only quantum entanglement provides perfect correlations in both photon position (near-field) and momentum (far-field) [6, 10], and suggested that this is crucial if both the image and the diffraction pattern are to be retrieved from the same source and leaving the object arm untouched [6]. Along the same line, recent experimental works [12, 13, 14], pointed out a momentum-position realization of the EPR paradox using entangled photon pairs produced by PDC. Based on this result, the Authors of [13, 14] argued that in ghost imaging schemes

entangled photons allows to achieve a better spatial resolution than any classically correlated beams, and in particular set a lower limit to the product of the resolutions of the images formed in the near and in the far-field of a given, single, classical source.

This claim is quite in contrast with the theoretical analyses of [7], where some of us proposed a particular source of classically correlated beams, that can emulate the behaviour of entangled beams in all the relevant aspects of ghost imaging, including the resolution capabilities. The proposed scheme relied on the use of two beams obtained by dividing on a beam splitter an intense beam with a thermal-like statistics. The two outcoming beams were shown to have strong, although completely classical, spatial correlations simultaneously in the near and in the far-field planes. Thanks to this, the scheme is able to reproduce all the results of ghost imaging with entangled beams, and numerical simulations confirmed this. In this paper we provide the first – to our knowledge – experimental evidence of the theoretical results obtained there. We show that both the ghost image and the ghost diffraction results emerge from the correlation measurements, that we may pass from one to the other by solely operating on the setup in the reference arm, and that the product of the resolutions clearly overcomes the limit set in [13, 14]. This definitively demonstrates that entanglement is not necessary for ghost imaging.

The experimental setup is sketched in Fig.1. The source of thermal light is provided by a slowly rotating ground glass placed in front of a scattering cell containing a highly turbid solution of $3\mu\text{m}$ latex spheres. When this is shined with a large collimated laser beam ($\lambda = 0.6328\mu\text{m}$, diameter $D_0 \approx 10\text{ mm}$), the stochastic interference of the waves emerging from the source produces a time-dependent speckle pattern characterized by a correlation time τ_{coh} on the order of 1s. The latter is associated to particle motion and can be tuned by varying the turbidity of the solution. A small portion of the speckle pattern is selected by a $D = 3\text{ mm}$ diaphragm at a distance $z_0 = 400\text{ mm}$ from the thermal source. The diaphragm realizes an angular selection of the pattern

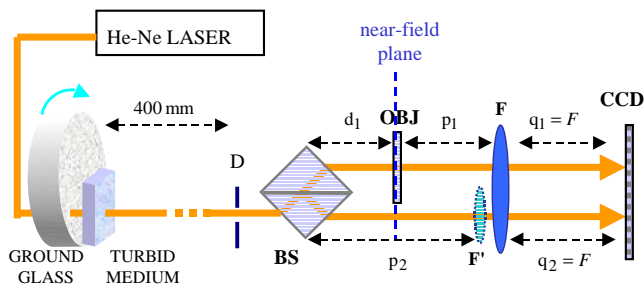


FIG. 1: Scheme of the setup of the experiment (see text for details).

allowing the formation of an almost collimated speckle beam characterized by chaotic statistics [15] and by speckles of size $\Delta x \approx \lambda z_0 / D_0 \approx 25 \mu\text{m}$ [15]. The speckle beam is separated by the beam splitter (BS) into "twin" speckle beams, that exhibit a high (although classical) level of spatial correlation. The two beams emerging from the BS have slightly non-collinear propagation directions, and illuminate two different non overlapping portions of the charged-coupled-device (CCD) camera. The data are acquired with an exposure time (1 ms) much shorter than τ_{coh} , allowing the recording of high contrast speckle patterns. The frames are grabbed at a rate of 1 Hz, so that each data acquisition corresponds to uncorrelated speckle patterns.

The optical setup of the object arm 1 is fixed. An object, consisting of a thin needle of $160 \mu\text{m}$ diameter inside a rectangular aperture $690 \mu\text{m}$ wide, is placed in this arm at a distance d_1 from the BS. A single lens of focal length $F = 80 \text{ mm}$ is placed after the object, at a distance p_1 from the object and $q_1 = F$ from the CCD. In this way the CCD images the far-field plane with respect to the object. However, the light being incoherent, the diffraction pattern of the object is not visible (nor its image, in this setup), in the intensity distribution of the object beam on the CCD, as shown by Fig.3a. We consider two different setups for the reference arm 2. In the first one, an additional lens of focal length F' is inserted in the reference arm immediately before the lens F . The total focal length F_2 of the two-lens system is smaller than its distance from the CCD $q_2 = F$, being $\frac{1}{F_2} \approx \frac{1}{F} + \frac{1}{F'}$. This allowed us to locate the position of the plane conjugate to the detection plane, by temporarily inserting the object in the reference arm and illuminating it with the laser light. After having determined the position of the object that produced a well focussed image on the CCD (image shown in Fig.2b), the object was translated in the object arm. The distances in the reference arm approximately obey a thin lens equation of the form $1/(p_2 - d_1) + 1/q_2 \approx 1/F_2$ [16]. The data of the intensity distribution of the reference arm are acquired and each pixel is correlated with the total photon counts of the object arm (i.e. with the sum of the photocounts

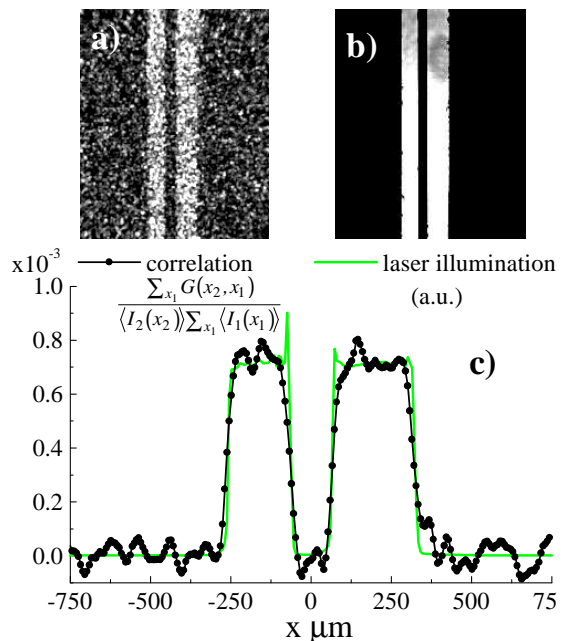


FIG. 2: Reconstruction of the object image via correlation measurements (Fig.1, with the lens F' inserted). (a) The intensity distribution of the reference arm is cross-correlated with the total photocounts in the object arm (statistics over 5000 CCD frames); (b) image observed by shining the laser light on the object. (d) The averages of 500 horizontal sections of the images shown in (a)(circles), and (b) (full line)

over a proper set of the pixels in the object arm), which corresponds to having a "bucket" detector in arm 1. Averages performed over few thousands of data acquisitions are enough to show a well-resolved reproduction of the image of the needle. This is shown in Fig.2a and can be compared with the image obtained by illuminating the object with the laser light (Fig.2b). Fig.2c plots the horizontal sections of the needle image as obtained via correlation (circles) and with the laser illumination (light full line), after averaging over 500 pixels in the vertical direction (exploiting the vertical symmetry of the image). The spatial resolution shown by correlated imaging with incoherent light is comparable with that obtained via coherent illumination.

In the second setup, without changing anything in the object arm, the lens F' is removed from the scheme of Fig.1, so that the reference beam passes through a single lens of focal F , placed at a distance $q_2 = F$ from the CCD. The spatial cross-correlation function of the reference and test arm intensity distributions is calculated by making averages over few hundreds of independent data acquisitions, and shows a sharp reproduction of the diffraction pattern of the object (Fig.3b). This is comparable with the diffraction pattern obtained by illuminating the object with the laser light (Fig.3c) (hence, by simply removing the scattering media and observing the light distribution

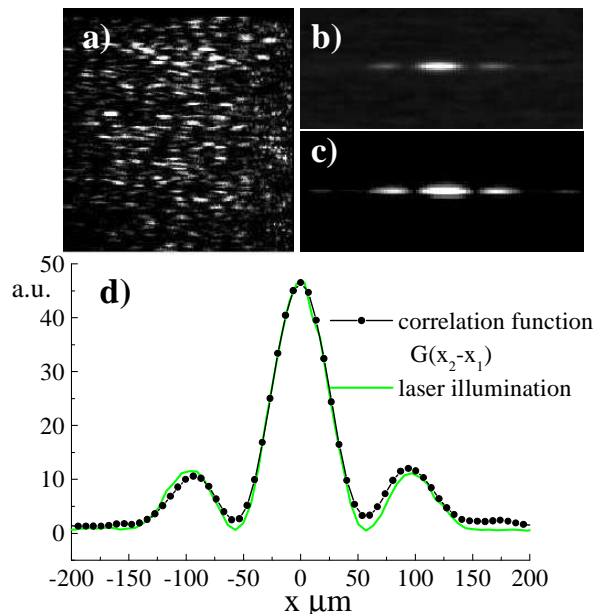


FIG. 3: Reconstruction of the diffraction pattern via correlation measurements (Fig.1, with the lens F' removed). (a) Single-shot intensity distribution in the object arm, showing no diffraction pattern. (b) Cross-correlation of the object-reference intensity distributions as a function of $\vec{x}_2 - \vec{x}_1$ (statistics over 500 frames); (c) diffraction pattern observed by shining the laser light on the object. (d) Horizontal sections of the diffraction patterns shown in (b) (dotted) plotted as a function of $x = x_2 - x_1$, and (c) (full line)

of the object arm on the CCD). Horizontal sections of these diffraction patterns are plotted in Fig. 3d, and shows basically that the spatial correlation measurement of the speckle beams offers a perfect reproduction of the diffraction pattern of this object. Notice that at difference from the ghost image experiment a spatial average is also involved, which improves the convergence rate as described in detail in [9].

Thus, in this way a high-resolution reconstruction of both the image and the diffraction pattern of the object have been performed by only operating on the optical setup of the reference arm and by using a single classical source.

The basic theory behind the setup shown in Fig. 1 has been explained in detail in Ref. [7]. The starting point is the input-output relations of a beam splitter

$$b_1(\vec{x}) = ta(\vec{x}) + rv(\vec{x}), b_2(\vec{x}) = ra(\vec{x}) + tv(\vec{x}) \quad (1)$$

where b_1 and b_2 are the object and reference beams emerging from the BS, t and r are the transmission and reflection coefficients of the BS, a is the speckle field and v is a vacuum field uncorrelated from a . The state of a is a thermal mixture, characterized by a Gaussian field statistics, in which any correlation function of arbitrary order is expressed via the second order correlation func-

tion

$$\Gamma(\vec{x}, \vec{x}') = \langle a^\dagger(\vec{x})a(\vec{x}') \rangle \quad (2)$$

The object information is extracted by measuring the spatial correlation function of the intensities $\langle I_1(\vec{x}_1)I_2(\vec{x}_2) \rangle$, where $I_i(\vec{x}_i)$ are operators associated to the number of photocounts over the CCD pixel located at \vec{x}_i in the i -th beam, and from this calculating the correlation function of intensity fluctuations

$$G(\vec{x}_1, \vec{x}_2) = \langle I_1(\vec{x}_1)I_2(\vec{x}_2) \rangle - \langle I_1(\vec{x}_1) \rangle \langle I_2(\vec{x}_2) \rangle. \quad (3)$$

The main result obtained in [7] was

$$G(\vec{x}_1, \vec{x}_2) = |tr|^2 \left| \int d\vec{x}'_1 \int d\vec{x}'_2 h_1^*(\vec{x}_1, \vec{x}'_1) h_2(\vec{x}_2, \vec{x}'_2) \Gamma(\vec{x}, \vec{x}') \right|^2, \quad (4)$$

where h_1 and h_2 are the impulse response function describing the optical setups in the two arms. Let us consider the scheme shown in Fig.1. The beams b_1 and b_2 follow identical paths from the BS to the object plane, which we shall refer to as the *near-field plane*. Due to the linearity of the BS transformation, the two beams at the near-field plane can be expressed via the same transformation as (1), with the a replaced by the speckle field which has propagated from the source to the near-field. In other words, our setup is equivalent to a setup where the physical BS is replaced by a point-like beam splitter performing the transformation (1) immediately before the object.

The setup of arm 1 is fixed, and by denoting with $T(\vec{x})$ the object transmission function, $h_1(\vec{x}_1, \vec{x}'_1) = (i\lambda F)^{-1} e^{-\frac{2\pi i}{\lambda F} \vec{x}_1 \cdot \vec{x}'_1} T(\vec{x}'_1)$. In the ghost image setup (Fig.1 with the lens F' inserted), the detection plane of the reference arm is the conjugate plane with respect to the near-field plane. Hence, apart from inessential phase factors $h_2(\vec{x}_2, \vec{x}'_2) = m\delta(m\vec{x}_2 + \vec{x}'_2)$, where $m \approx 1.2$ is the magnification factor of the two-lens system. Inserting this in Eq. (4):

$$G(\vec{x}_1, \vec{x}_2) \propto \left| \int d\vec{x}'_1 \Gamma_n(\vec{x}'_1, -m\vec{x}_2) T^*(\vec{x}'_1) e^{i\frac{2\pi}{\lambda F} \vec{x}_1 \cdot \vec{x}'_1} \right|^2 \quad (5)$$

$$\approx |T(-m\vec{x}_2)|^2 \left| \int d\vec{x}'_1 \Gamma_n(\vec{x}'_1, -m\vec{x}_2) e^{i\frac{2\pi}{\lambda F} \vec{x}_1 \cdot \vec{x}'_1} \right|^2 \quad (6)$$

where $\Gamma_n(\vec{x}, \vec{x}')$ is the second order field correlation function (2) of the speckle beam in the near-field. The second line of Eq.(6) was derived under the assumption that the smallest scale over which the object changes is larger than the length over which $\Gamma_n(\vec{x} - \vec{x}')$ decays, which we shall refer to as the *near-field coherence length* Δx_n . In general the result of a measurement of G in this setup is a convolution of the object transmission function with the near field correlation function Γ_n , so that that Δx_n sets the spatial resolution for the reconstruction of the image. Note that in the ghost image experiment a bucket detection scheme is employed in arm 1, so what we observe in

Fig.2a is $\int d\vec{x}_1 G(\vec{x}_1, \vec{x}_2)$, which makes the imaging incoherent [9].

In the ghost diffraction experiment we simply remove the lens F' from the setup of Fig.1, so that the detection plane of beam 2 is in the focal plane of the lens F . Hence, $h_2(\vec{x}_2, \vec{x}'_2) = (i\lambda F)^{-1} e^{-\frac{2\pi i}{\lambda F} \vec{x}_2 \cdot \vec{x}'_2}$. From Eq.(4), we obtain

$$G(\vec{x}_1, \vec{x}_2) \propto \left| \int d\vec{\xi} \vec{\Gamma}_f(\vec{\xi}, \vec{x}_2) \tilde{T}^* \left[(\vec{x}_1 - \vec{\xi}) \frac{2\pi}{\lambda F} \right] \right|^2 \quad (7)$$

$$\approx \left| \tilde{T} \left[(\vec{x}_1 - \vec{x}_2) \frac{2\pi}{\lambda F} \right] \right|^2 \left| \int d\vec{\xi} \vec{\Gamma}_f(\vec{\xi}, \vec{x}_2) \right|^2, \quad (8)$$

where $\tilde{T}(\vec{q}) = \int \frac{d\vec{x}}{2\pi} e^{-i\vec{q} \cdot \vec{x}} T(\vec{x})$ is the amplitude of the diffraction pattern from the object. $\Gamma_f(\vec{x}, \vec{x}')$ is the second order correlation function (2) of the speckle field in the far-field plane, as observed in the focal plane of the lens F ; its correlation length Δx_f (the *far-field coherence length*) sets the limit for the spatial resolution of the diffraction pattern reconstruction.

Relevant to the resolution of the ghost imaging and ghost diffraction schemes are hence the spatial coherence properties of the speckle field in the near field immediately before the object, and in the far-field plane. These can be investigated by measuring the fourth-order correlation functions, in the absence of the object. In the near-field plane, we measured the spatial auto-correlation function of the reference beam $\langle I_2(\vec{x}) I_2(\vec{x}') \rangle$ in the setup with the lens F' inserted, so that the reference beam recorded by the CCD is the (demagnified) image of the near-field. This is plotted in Fig.4 (squares) as a function of $|\vec{x} - \vec{x}'|$. Neglecting the small shot noise contribution

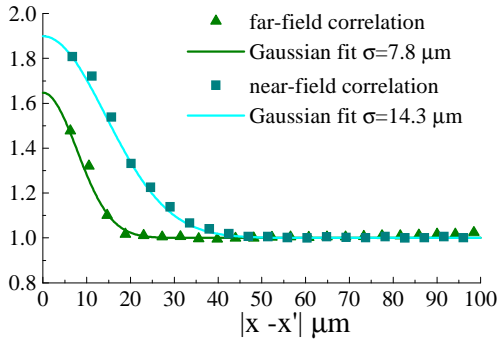


FIG. 4: Fourth order auto-correlation function in the near field plane (squares) and in the far-field plane (triangles). The full lines are Gaussian fits of the correlation peaks, and the data have been normalized to the baseline values.

at $\vec{x} = \vec{x}'$, by using Siegert formula for Gaussian field statistics and the BS transformation (1),

$$\begin{aligned} \langle I_2(\vec{x}) I_2(\vec{x}') \rangle &- \langle I_2(\vec{x}) \rangle \langle I_2(\vec{x}') \rangle \\ &= \left| \langle b_2^\dagger(\vec{x}) b_2(\vec{x}') \rangle \right|^2 = |r|^4 |\Gamma_n(m\vec{x}, m\vec{x}')|^2 \end{aligned} \quad (9)$$

The baseline in Fig.4 corresponds to the product of mean intensities, while the narrow peak at $\vec{x} = \vec{x}'$ is the r.h.s

of (9), and reflects the spatial coherence properties of the field. By making a Gaussian fit of this peak we obtained a variance $\sigma_n = 14.3 \mu\text{m}$. From this we can infer the coherence length in the near-field plane, as $\Delta x_n \approx 2m\sigma_n = 34.3 \mu\text{m}$. The triangles in Fig.4 plot the intensity correlation function in the far-field plane, obtained by measuring the auto-correlation function of beam 1 in the focal plane of the lens F . The narrow peak in this plot is now $|t|^4 |\Gamma_f(\vec{x}, \vec{x}')|^2$ and reflects the spatial coherence properties of the speckles in the far-field plane. Its variance calculated by means of a Gaussian fit is $\sigma_f = 7.8 \mu\text{m}$, from which we infer a far-field coherence length $\Delta x_n = 2\sigma_f = 15.6 \mu\text{m}$. This in turn corresponds to a spread in transverse wave vectors $\Delta q = \frac{2\pi}{\lambda F} \Delta x_f = 1.93 \times 10^{-3} \mu\text{m}^{-1}$

In the spirit of the EPR argument brought forward by [13, 14], we find a product of the near-field and far-field resolutions

$$\Delta x_n \Delta q = 0.066 \quad (10)$$

which is by far smaller than the limit of unity imposed by EPR-like arguments in [13, 14], and is at least four times smaller than the results there reported, where entangled photons were used to retrieve the ghost image and the ghost diffraction pattern.

Notice that there is no violation of any EPR bound for such a separable mixture. In fact, in any plane, the conditional probability of detecting a photon at position \vec{x}_2 in beam 2 given that a photon was detected at position \vec{x}_1 in beam 1 is:

$$P(\vec{x}_2 | \vec{x}_1) \propto \frac{\langle I_2(\vec{x}_2) I_1(\vec{x}_1) \rangle}{\langle I_1(\vec{x}_1) \rangle} = \langle I_2(\vec{x}_2) \rangle + |tr|^2 \frac{|\Gamma(\vec{x}_1, \vec{x}_2)|^2}{\langle I_1(\vec{x}_1) \rangle} \quad (11)$$

Hence, given that photon 1 was detected at \vec{x}_1 there is a large probability of detecting a photon anywhere in beam 2 (the first term at r.h.s. of Eq. (11)), with a narrow probability peak localized at $\vec{x}_2 = \vec{x}_1$. Thanks to the first term, there is no non-locality ingredient in the correlation of the classical speckle beams, as obviously must be. However, the crucial point is that the resolution of imaging schemes based on correlation measurements depends only on the widths of the peaks in Fig. 4, and that their product in the near and in the far field are not bounded by any EPR-like inequality. As a matter of fact the near and the far field coherence lengths, corresponding roughly to the size of the speckles in the near and in the far-field, are independent quantities. In the near field, the size of the speckle depends on the laser diameter D_0 , and from the total optical path length z from the source to the near-field plane, $\Delta x_n \propto \lambda z / D_0$ [15]. The pinhole D being rather close to the near-field plane, we checked that the speckle size in this plane did not depend on the pinhole aperture. The pinhole aperture instead influences the size of the speckles in the far field, this being roughly given by $\Delta x_f \propto \lambda F / D$ [15]. Using the values

of our setup, we find $\Delta x_n \approx 30 \mu m$ and $\Delta x_f \approx 17 \mu m$, in good agreement with the values estimated from the correlation (Fig. 4).

In conclusion, we have reported on an experimental demonstration of high resolution ghost imaging and ghost diffraction by using a single source of classically correlated thermal light. The distributed imaging character of our experiment is evident from the fact that the information on the object spatial distribution can be processed by only acting on the reference beam 2 (e.g. passing from the image to the diffraction pattern). The product of resolutions of the ghost image and the ghost diffraction schemes is well below the limit that was claimed by former literature to be achievable only with entangled beams. This could be further improved by optimizing the scheme (e.g. with a larger pinhole, a larger laser diameter) which was constrained in our experiment by the need of using a single CCD and a low-power laser. This definitely proves the claim set forth in [7], that the only advantage of entanglement with respect to classical correlation lies in the better visibility of information. This might be useful in very high sensitivity measurement or in quantum information schemes, where e.g. the information need to be hidden to a third party, but does not give any evident practical advantage when attempting to process information from a macroscopic classical object, as in the experiment shown here.

This work was carried out in the framework of the project QUANTIM of the EU, of the PRIN project of MIUR "Theoretical study of novel devices based on quantum entanglement", and of the INTAS project "Non-classical light in quantum imaging and continuous variable quantum channels". M.B. acknowledges financial support from the Danish Technical Research Council (STVF) and the Carlsberg Foundation.

-
- [1] T. B. Pittman, Y. H. Shih, D. V. Strekalov, and A. V. Sergienko, *Phys. Rev. A* **52**, R3429 (1995).
 - [2] D. V. Strekalov, A. V. Sergienko, D. N. Klyshko, and Y. H. Shih, *Phys. Rev. Lett.* **74**, 3600 (1995).
 - [3] P. H. Souto Ribeiro, S. Padua, J. C. Machado da Silva, and G. A. Barbosa, *Phys. Rev. A* **49**, 4176 (1994).
 - [4] A. F. Abouraddy, B. E. A. Saleh, A. V. Sergienko, and M. C. Teich, *Phys. Rev. Lett.* **87**, 123602 (2001).
 - [5] A. F. Abouraddy, B. E. A. Saleh, A. V. Sergienko, and M. C. Teich, *J. Opt. Soc. Amer. B* **19**, 1174 (2002).
 - [6] A. Gatti, E. Brambilla, and L. A. Lugiato, *Phys. Rev. Lett.* **90**, 133603 (2003).
 - [7] A. Gatti, E. Brambilla, M. Bache, and L. A. Lugiato, *Phys. Rev. A* **70**, 013802 (2004); *Phys. Rev. Lett.*, in press; quant-ph/0307187
 - [8] M. Bache, E. Brambilla, A. Gatti, and L. A. Lugiato, *Phys. Rev. A*, in pres; quant-ph/0402160 (2004).
 - [9] M. Bache, E. Brambilla, A. Gatti, and L. A. Lugiato, In preparation (2004).
 - [10] E. Brambilla, A. Gatti, M. Bache, and L. A. Lugiato, *Phys. Rev. A* **69**, 023802 (2004).
 - [11] R. S. Bennink, S. J. Bentley, and R. W. Boyd, *Phys. Rev. Lett.* **89**, 113601 (2002).
 - [12] J. C. Howell, R. S. Bennink, S. J. Bentley, R. W. Boyd, *Phys. Rev. Lett.* **92**, 210403 (2004).
 - [13] R. S. Bennink, S. J. Bentley, R. W. Boyd, and J. C. Howell, *Phys. Rev. Lett.* **92**, 033601 (2004).
 - [14] M. D'Angelo, Y-H Kim, S.P. Kulik, and Y. Shih, *Phys. Rev. Lett.* **92**, 233601 (2004).
 - [15] J. W. Goodman, in *Laser speckle and related phenomena*, edited by J. C. Dainty (Springer, Berlin, 1975), vol. 9 of *Topics in Applied Physics*, p. 9.
 - [16] This is only approximately true because the two-lens system is equivalent to a thick lens rather than a thin lens.